Article

MMS

Mathematics and Mechanics of Solids
2015, Vol. 20(6) 697–720

DOI: 10.1177/1081286514551504
mms.sagepub.com

SAGE

Nonaffine response of skeletal muscles on the 'descending limb'

Igor Novak
Department of Cell Biology, University of Connecticut, Farmington, CT USA

Lev Truskinovsky
Laboratoire de Mechanique des Solides, Ecole Polytechnique, Palaiseau, France

Received 6 June 2014; accepted 16 June 2014

Abstract
Tetanized muscle myofibrils are often modeled as one-dimensional chains where springs represent half-sarcomeres (HS). The force–length relation for individual HSs (isometric tetanus) is known to have a 'descending limb', a segment with an apparently negative stiffness. Despite the potential mechanical instability on the descending limb, the isometric tetanus is usually interpreted as describing an *affine* deformation. At the same time, active stretching during tetanus around the descending limb is known to produce *non-affine* sarcomere patterns. In view of this paradox, the question whether the mechanical behavior of a myofibril can be interpreted as a response of a single contractile unit has been a subject of considerable controversy over the last 50 years. In this paper we question the claim that the isometric tetanus describes homogeneous configurations of the HS chain. To distinguish between the multitudes of non-affine equilibrium states available to this mechanical system, we propose to use the concept of a stored mechanical *energy*. While the notion of energy is natural from a mechanical point of view, physiologists have resisted it so far on the grounds that the contractile elements are *active*. We discuss how this objection can be overcome and show that the appropriately defined stored energy of a tetanized myofibril with N contractile units has exponentially many local minima. We then argue that the *ruggedness* of the ensuing energy landscape is responsible for the experimentally observed history dependence and hysteresis in the mechanical response of a tetanized muscle near the descending limb. A nonlocal extension of the chain model, accounting for surrounding tissues, shows that both the ground states and the marginally stable states are fine mixtures of short and long HSs. These mixtures are homogeneous at the macro-scale and inhomogeneous at the micro-scale and we show that the negative overall slope of the step-wise tetanus can coexist with a positive instantaneous stiffness. A salient feature of the nonlocal model is that the variation of the degree of non-uniformity with elongation follows a complete devil's staircase.

Keywords
muscle mechanics, half-sarcomere, descending limb, tetanus, myofibril.

1. Introduction

Although the general physiological and biochemical outlines of how the contractile mechanism of skeletal muscles operates are established, some fundamental details of mechanical nature remain to be

Dedicated to Ray Ogden with admiration

Corresponding author:
Lev Truskinovsky, Laboratoire de Mechanique des Solides, Ecole Polytechnique, Palaiseau 91128, France.
Email: trusk@lms.polytechnique.fr

clarified. In this paper we address a still controversial issue of muscle stability on the 'descending limb' of the force–length curve describing fully tetanized muscles [1-5].

We recall that a single muscle fiber is a three-dimensional network of linearly aligned and passively interlinked strings called myofibrils. An individual myofibril is a crystal-like system of repeating structural units (sarcomeres) each consisting of two mirrored force-generating subunits (half sarcomeres [HS]), see Figure 1. The active contraction inside individual HSs results from the relative sliding of myosin and actin myofilaments. The myofilaments interact through multiple myosin cross-bridges that protrude laterally from myosin and bind actin. In the nonequilibrium environment, the preferred locations of the attachment sites shift away from their equilibrium positions and stochastic binding stretches the elastic elements inside the cross-bridges producing a macroscopic force [6].

The maximal active force generated by a muscle in a hard (isometric) device depends on the number of pulling cross-bridge heads (motors), which is in turn controlled by the myofilament overlap. The overlap can be modified by the passive pre-stretch Δl and a large number of experimental studies were devoted to the measurement of the dependence of the maximum force on the pre-stretch $F(\Delta l)$ known as the isometric tetanus curve [7-11]. The isometric tetanus has been traditionally interpreted as a description of the *affine* deformation representing a direct readout of the geometrical arrangement at the microscale. In particular, it has been realized that a stretch beyond a certain limit would necessarily decrease the filament overlap and therefore the active component of $F(\Delta l)$ must contain a segment with a negative stiffness. While such active negative stiffness is partially compensated by the positive stiffness of parallel passive cross-linkers [12], for some skeletal muscles the total force–length relation $F(\Delta l)$ still has a range where the force decreases with elongation [13]. The resulting descending limb is illustrated in Figure 2.

A conventional interpretation of the isometric tetanus is based on the assumption that in a uniformly activated myofibril all HSs are operating identically. This assumption is analogous to what is known in solid mechanics as the Cauchy–Born (affinity) hypothesis. The potential instability of the Cauchy–Born (affine) configurations on the descending limb was first realized by Hill [14] and various aspects of this instability have been discussed extensively in the last 50 years, see [15-19] and the references cited therein.

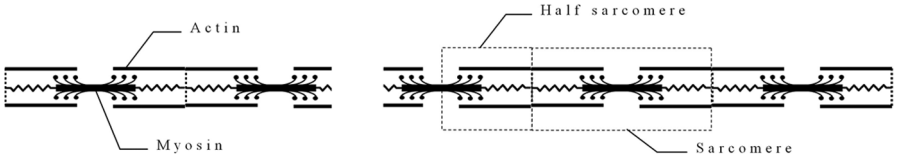

Figure 1. Schematic representation of a myofibril. Actin filaments are shown by thin lines and myosin filaments by thick lines with protruding cross-bridges. Passive parallel elements are shown as springs.

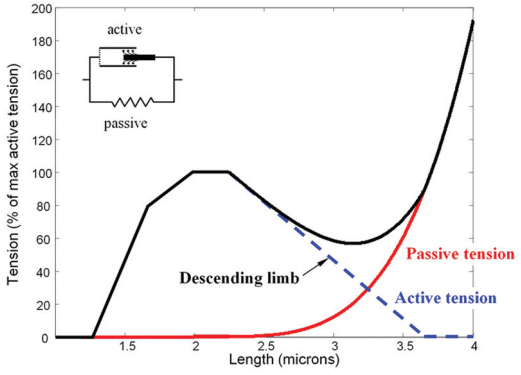

Figure 2. Schematic representation of the isometric tetanus curve for frog striated muscle. Active component is shown by a dashed line and passive component by a solid line. The descending limb is marked for the active force component only.

In continuum mechanics it has been also long understood that a softening material will necessarily experience (localization) instability [20, 21]. In terms of the observed quantities such instability would mean that on the descending limb any initial imperfection would cause a single myosin filament to be pulled away from the center of the activated HSs [22-27].

Some experiments seem to be indeed consistent with non-uniformity of different cross-linkers spacing and with random displacements of the thick filaments away from the centers of the sarcomeres [10, 28-31]. Notice that the non-affine HS length distribution can be sometimes disguised as increased disorder or skewing [32-34]. The softening-induced localization instability hypothesis is also compatible with the fact that progressive increase of the range of dispersion in HS lengths, associated with a slow rise of force during tetanus (creep phase), is observed mostly around the descending limb [24, 35–37].

An apparently related feature of the muscle response on the descending limb is the non-uniqueness of the isometric tension, which was shown to depend on the pathway through which the elongation is reached [38–49]. For instance, experiments demonstrate that when a muscle fiber is activated at a fixed length and then suddenly stretched while active, the tension first rises and then falls without reaching the value that the muscle generates when stimulated isometrically (residual force enhancement). Similar phenomena have been also observed during sudden shortening of the active muscle fibers. Thus, if a stimulated muscle is allowed to shorten to the prescribed length it develops less tension than during direct tetanization at the final length. It has been argued that the nonuniform (nonaffine) HS behavior plays a major role in such memory behavior [50]. For instance, the residual force enhancement is usually explained by the fact that asymmetric length changes within the two neighboring HSs result in greater myofilament overlap in one half of the sarcomere. The HSs with increased filament overlap are then able to produce a greater force than during affine deformation while weaker HSs are stabilized by the parallel passive elements.

Several *affine* mechanisms of residual force enhancement have been proposed as well, including those that involve the recruitment of additional force-generating elements [51–55] and those relying on the stiffening of the 'passive' parallel elastic elements (mostly titin molecules) as they reach the 'active' states of their own [56–60]. However, apparently none of these alternative explanations can account for the observed history dependence on the *quantitative* level [50, 61, 62].

The development of a nonaffine deformation on the descending limb have been thoroughly studied in the *dynamic* setting where it is usually assumed that an active element (tetanized HS) is a softening nonlinear elastic spring bundled with a dashpot characterized by a realistic (Hill–Katz) force–velocity relation [9, 26, 42, 63–65]. The dynamic models were shown to be compatible with the residual force enhancement after stretch and the associated deficit of tension after shortening, even though a variety of numerical tests demonstrated that around the descending limb the HS configuration becomes nonuniform at the time scale which is unrealistically long. The simulations, however, left unanswered the question about the fundamental origin of the *multi-validness* of the muscle response around the descending limb. Similarly, it remains unclear how the microscopic inhomogeneity (non-affinity) of the HS configuration can hide behind a largely homogenous response at the macro-level.

In an attempt to answer these questions we use the simplest representation of a muscle myofibril as a one-dimensional discrete chain with N 'softening' contractile units each reinforced by a parallel linear element. By following a similar study of the behavior of shape memory alloys [66] we show that an isometrically activated myofibril, viewed as mechanical system, has an exponentially large (in N) number of configurations with equilibrated forces. To distinguish between various nonaffine equilibrium states available to such a prototypical myofibril, we propose to use a notion of stored mechanical *energy*. While this notion is essential in mechanics, physiologists have so far resisted energetic interpretations of the mechanical equilibrium on the grounds that the contractile elements are *active*, mentioning correctly that the energy *flows* through them rather than being stored. We discuss how this objection can be overcome and show that the relevant energy should be attributed to the passive mechanical structures *inside* individual HSs. These structures are loaded both internally, by molecular motors, and externally, by applied forces and their mechanical energy can be readily computed. Finally we check that the dynamics induced by the conventional Hill–Katz kinetic model implies a local minimization of the so defined energy.

Our analysis of the chain model shows that the energy landscape of a tetanized myofibril is *rugged*. The possibility of a variety of evolutionary paths in such a landscape creates a potential for history

dependence and explains the mysteries of the 'permanent extra tension' and of the 'permanent deficit of tension' observed on the descending limb. We demonstrate that in the continuum limit the domain of metastability on the force–length plane is represented by a dense set of stable branches corresponding to states with a fixed degree of inhomogeneity and that the negative overall (apparent) slope of the force–length relation can be viewed as a combination of an infinite number of infinitesimal micro-steps with positive slopes. In the spirit of Allinger et al. [16] we claim that this 'coexistence' of the negative *averaged* stiffness with the positive *instantaneous* stiffness is the main factor responsible for the stable performance of the muscle fiber on the descending limb.

While the price of stability on the descending limb is the limited microscopic non-uniformity in the distribution of HS lengths, the locally non Cauchy–Born (non-affine) behavior may be still compatible with the uniformity in *average* at the scale of the whole myofibril [34]. To emphasize this point we propose a mechanism ensuring that the macroscopic configuration is a maximally fine mixture of long and short HSs. This mechanism involves long-range *mechanical signaling* between individual HSs via the surrounding elastic medium and we show that it brings into the model *competing interactions* with incommensurate length scales [67]. The resulting ground states are homogeneous at the macro-scale and inhomogeneous at the micro-scale, which explains why the nonaffine nature of the tetanized configurations on the descending limb is so difficult to capture in the experiment. An intriguing feature of the proposed nonlocal extension of the chain model of a myofibril is that the variation of the degree of non-uniformity with elongation follows a complete devil's staircase.

The rest of the paper is divided into two main sections. In Section 2 we study the conventional *local* model of a muscle myofibril and in Section 3 we analyze a *nonlocal* generalization of this model. We begin Section 2 by introducing the notion of a softening active spring and discuss the microscopic origin of the descending limb in the response of an individual tetanized HS. Then we study the mechanical behavior of a collection of HSs arranged in series and explore the multiplicity of the configurations with equilibrated forces. The use of an energetic framework allows us to study stability of the configurations and distinguish between locally and globally stables states. In Section 3 we introduce a nonlocal version of the chain model allowing us to clarify the origin of the macroscopic homogeneity of the microscopically nonaffine patterns around the descending limb. Section 4 contains our main conclusions and mentions some open problems.

2. The local model

In this section we study the simplest mechanical representation of a muscle myofibril as a chain of N identical sarcomeres. Since the thick filaments can move off the center of the sarcomere, it is natural to view a single sarcomere as a pair of identical HSs, see Figure 1. Therefore, we substitute the original chain by an equivalent one with $N = 2n$ contractile units separated by massless nodes.

2.1. Mechanical description of a single HS

Suppose that u_i is a displacement of the ith point separating two neighboring contractile units. Then $\Delta l_i = u_i - u_{i-1}$ is the elongation of the corresponding HS and we assume that it is characterized by a force–length relation $F(\Delta l)$. Since the passive element is connected in parallel with the active component, see Figure 2, we can write $F(\Delta l) = F_p(\Delta l) + F_a(\Delta l)$, where $F_p(\Delta l)$ is the passive force and $F_a(\Delta l)$ is the active force.

The passive force is almost absent in the (floppy) physiological range and its main function is to provide support in the case of the accidental overstretch beyond the acto-myosin overlap. Despite such strong nonlinearity it will be convenient to begin by representing the passive element as a linear elastic spring with the force–length relation of the form $F_p(\Delta l) = E_3 \Delta l / a$. Here E_3 is the elastic modulus and a is the reference length. In what follows we neglect viscoelastic properties of the passive elements even though their role in the heterogeneous *dynamics* of a myofibril may be substantial [23]. We also do not take into account that the passive structural protein titin becomes stiffer upon activation due to calcium binding or due to its own binding to actin which suggests that active stretch encounters a stiff passive element even when passive stretch does not [60].

The assumption that the *active* behavior of a tetanized HS can be modeled by a *material* constitutive relation $F_a(\Delta l)$ is already controversial. Indeed, active force is known to be generated by a complex micro-machinery involving stochastically fluctuating components, continuous supply of energy and dissipation (e.g. [68, 69]). The active force is ultimately produced by stretched internal *springs* that are loaded endogenously by molecular motors. A task of recovery of the *constitutive* description of such elements from observations is complicated by the fact that experiments describe the collective behavior of a number of HSs and the mechanical data are obtained through a very particular protocol involving activation at a fixed length rather than continuous deformation.

By making an assumption that the function $F_a(\Delta l)$ describes the constitutive response of a quasi-elastic element we, first of all, implicitly assume that at the time scale of interest the microscopic dynamical processes (ensuring active force generation) are instantaneous and that the corresponding microscopic degrees of freedom can be adiabatically eliminated [64]. The elimination of fast time scales means significant simplification of the formalism, however, it also prevents one from capturing the response of the system at fast loading rates. In particular, we lose, even if only at a scale of a single HS, the instantaneous stiffness on the descending limb discussed in [15–19]. The *adiabatic* model of a HS also misrepresents the potentially nonaffine microscopic dynamics of molecular motors at sub-HS level which was recently shown to contribute to the residual force enhancement [27].

According to the sliding filament theory the tetanus curve must be compatible with the existence of three different structural arrangements of myofilaments. First, it must account for the fact that on the ascending limb a partial overlap of actin filaments from different families contributes to mutual 'neutralization' of some of the active cross-bridges making them 'non-force-bearing'. Since such a detrimental actin overlap diminishes with stretching, the active force generated by the force-bearing cross-bridges increases with Δl and in view of its geometric origin this augmentation of the force is almost linear. The ascending limb ends with a plateau where the number of force bearing cross-bridges remains constant while the actual binding sites are changing. At the scale of a single HS, the interval of Δl corresponding to such a 'reversible plasticity' is rather short and can be neglected. Therefore, we assume that the ascending limb is followed directly by the descending limb, where the diminishing overlap of actin and myosin filaments leads to the gradual decrease of the number of the force bearing cross-bridges due to what one can call a 'reversible damage'. More specifically, we assume that since all bound cross-bridges contribute equally to active force generation, and since stretching beyond the range of an optimal overlap leads to the loss of attachment, the active force decreases linearly with the number of remaining pullers. The descending limb is expectedly followed by a zero-activity regime where there is no overlap of actin and myosin filaments and the active force cannot be generated.

In view of this reasoning and in an attempt to simplify computations we adopt a highly schematic trilinear approximation for the active force–length relation

$$F_a(\Delta l) = \begin{cases} E_1 \dfrac{\Delta l}{a} & , \quad \Delta l \le a_1 \\ -E_2 \dfrac{\Delta l - a_2}{a} & , \quad a_1 < \Delta l < a_2 \\ 0 & , \quad \Delta l \ge a_2 \end{cases}$$

where due to the continuity, $E_2 = a_1 E_1/(a_2 - a_1)$. The overall force–length relation for a parallel *bundle* of active and passive elements has then an up–down–up form characteristic of a material undergoing structural transformation [66]. This is illustrated in Figure 3 where we use dimensionless variables $\varepsilon = \Delta l/a_1$ and $f(\varepsilon) = aF(\Delta l)/(E_1 a_1)$; in view of the above analogy we refer to the three distinct branches of the force–length relation $f(\varepsilon)$ as phases *I, II*, and *III*.

2.2. The mechanical behavior of a HS chain

Consider now the behavior of N individual HSs connected in series (see Figure 4). Suppose that the myofibril is loaded isometrically so that the controlling parameter is the total strain $\bar{\varepsilon}$. To find the equilibrium configurations available to this mechanical system we need to solve the force balance equations

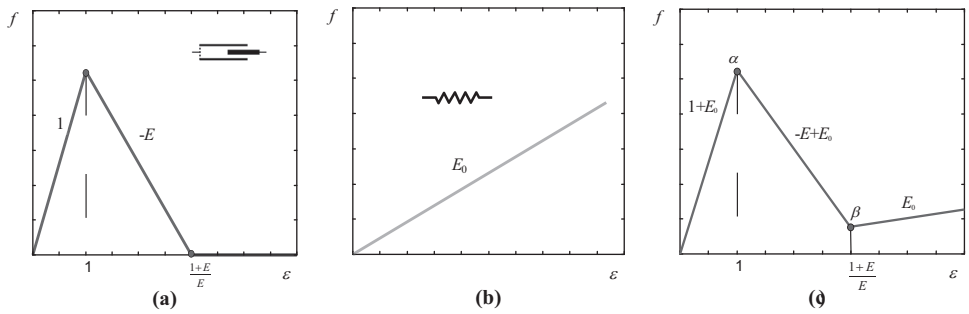

Figure 3. Non-dimensional force–strain relations for an active component (a), a passive elastic component (b) and for active and passive component grouped into a parallel bundle (c). The dimensionless parameters are $E = a_1/(a_2 - a_1)$ and $E_0 = E_3/E_1$.

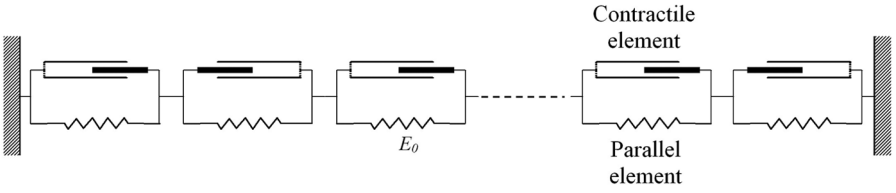

Figure 4. A muscle fiber modeled as a chain of HSs; each HS is a parallel bundle of an active contractile element and a passive linear elastic element.

$$f(\varepsilon_i) = \bar{f}, \quad i = 1, ..., N, \tag{1}$$

where $\bar{f}$ represents the constant force in the fiber. These equations may have up to three different solutions corresponding to three different phases

$$\varepsilon_I = \frac{\bar{f}}{1+E_0}, \varepsilon_{II} = -\frac{\bar{f}}{E-E_0} + \frac{1+E}{E-E_0}, \varepsilon_{III} = \frac{\bar{f}}{E_0}. \tag{2}$$

Given that the model is invariant under permutations it is natural to arrange all solutions of (2) into equivalence classes, labeled by the triples (k,l,m) specifying the number of springs in each of the phases. In what follows we also use phase fractions $x = k/N, y = l/N, z = m/N$.

For the phase configuration (k,l,m) the average strain is $N\bar{\varepsilon} = k\varepsilon_I(\bar{f}) + l\varepsilon_{II}(\bar{f}) + m\varepsilon_{III}(\bar{f})$. By inverting this relation and using (2) we obtain for each phase configuration its own macroscopic force–strain relation:

$$\bar{f}(\bar{\varepsilon}) = E_*(\bar{\varepsilon} - \varepsilon_*),$$

where

$$\varepsilon_* = \frac{y(1+E)}{E-E_0}, E_* = \frac{E_0(1+E_0)}{z+E_0(1-\varepsilon_*)}.$$

To illustrate the multiplicity of the equilibrium states in this mechanical system, we present in Figure 5 the case of two full sarcomeres in series ($N = 4$). Since in the realistic myofibril $N \sim 10^4$ it is also of interest to study the continuum limit $N \to \infty$. One can show that in this limit the equilibria fill densely the domain bounded by the four lines: $\bar{f} = (1+E_0)\bar{\varepsilon}$, $\bar{f} = E_0\bar{\varepsilon}$, $\bar{f} = f_{\max} = 1+E_0$, and $\bar{f} = f_{\min} = E_0(1+E)/E$, see Figure 6.

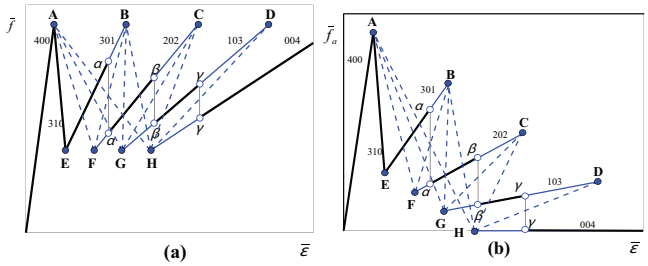

Figure 5. Mechanical response of the simplest myofibril containing two sarcomeres in series ($N = 4$, $E = 0.3$, $E_0 = 0.1$): (a) the total force $\bar{f}(\bar{\varepsilon})$; (b) the active force $\bar{f}_a(\bar{\varepsilon}) = \bar{f}(\bar{\varepsilon}) - E_0\bar{\varepsilon}$. The numbers indicate phase configurations (k, l, m). Points **A, B, C, D** and **E, F, G, H** indicate limits of stability. The global minima of the energy are shown with a bold line (path **AE αβγ**), the metastable states with solid lines, the unstable states with dashed lines.

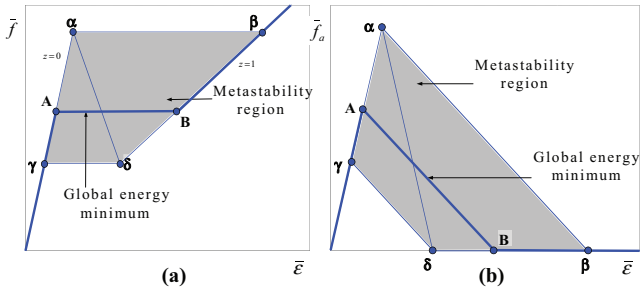

Figure 6. Mechanical behavior of a myofibril in the continuum limit: (a) the total force $\bar{f}(\bar{\varepsilon})$; (b) the active force $\bar{f}_a(\bar{\varepsilon}) = \bar{f}(\bar{\varepsilon}) - E_0\bar{\varepsilon}$. Parameters: $E = 1$, $E_0 = 0.25$. Global minimum of the energy is shown with a bold line **(γABδ)**. Points in the shaded domain **(γ, α, β, δ)** correspond to metastable configurations. Lines **(α, β)** and **(γ, δ)** correspond to marginally stable states.

From Figure 6 it is clear that due to the large number of micro-configurations with balanced forces, the outcome of an experiment with a finite stretch applied to a pre-activated myofibril cannot be predicted from the force balance equations only. Instead, the response of a tetanized myofibril depends on the particularities of the stochastic dynamics at the microscale. To avoid the microscale analysis, it is often assumed that each HS is equipped with a macroscopic force–velocity relation describing a steady-state shortening in isotonic tests [63, 70, 71]. This is equivalent to an assumption that we attach in parallel to the bundle of active and passive units a damping element of a frictional type. Then, if f is the external force acting on a HS, we can write $f = f(\varepsilon) + \phi(\varepsilon, \dot{\varepsilon})$ where the second term on the right describes the dissipative force. Instead of the actual Hill–Katz-type expression for this force we use in what follows a much simpler linear approximation $\phi(\dot{\varepsilon}) = \mu^{-1}\dot{\varepsilon}$, where $\mu > 0$ is the mobility coefficient, which preserves the main features of a more realistic kinetic model.

It is clear that the linear dynamics is fully compatible with the fact that the homogeneous states on the two ascending limbs of the force–length relation $f(\varepsilon)$ are stable while the homogeneous states on the descending limb are unstable. In Figure 7, we illustrate the final states reached from various initial homogeneous (affine) configurations on the descending limb: the system eventually gets trapped in an inhomogeneous (nonaffine) equilibrium configuration. From Figure 7, we see that, on the average, the (apparent) slope of the resulting jagged force–length curve is negative.

2.3. Energy minimization as a selection criterion

We have seen that by using a gradient-flow-type dynamic extension of the equilibrium model we can obtain a particular way of selecting among the multiplicity of the available equilibrium states. Such an over-damped dynamics leads to the local *energy minimization* because the associated rate of dissipation

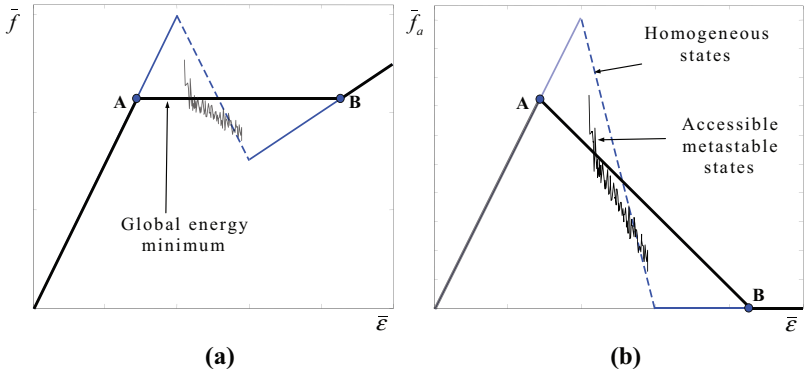

Figure 7. Numerical simulations showing selected non-affine metastable states (jagged line) that are accessible from the homogeneous configuration through the gradient flow dynamics $\phi(\dot{\varepsilon}) = \mu^{-1}\dot{\varepsilon}$. Starting points in these dynamic experiments with the fixed average strain $\bar{\varepsilon}$ were affine configurations on the descending limb (dashed line). The segment **AB** corresponds to the global minimum of the energy. Parameters: $E = 2$, $E_0 = 0.5$.

$$D(\varepsilon, \dot{\varepsilon}) = \sum_{i=1}^{N} \phi(\varepsilon_i, \dot{\varepsilon}_i)\dot{\varepsilon}_i = \mu^{-1} \sum_{i=1}^{N} \dot{\varepsilon}_i^2$$

is positive definite. The question arises whether the concept of energy is meaningful at all in the context of active systems. We know that to generate active force the motors must receive and dissipate energy, which implies that the energy *flows* through the system. This is obviously not the energy we need to account for.

In search of the place where energy can be *stored*, we observe that each HS has its own passive mechanical machinery loaded *endogenously* by molecular motors. In the state of tetanus some energy is stored in these passive structures. To change the amount of this energy one needs to arrange a transition from one active state to another. Suppose that in order to make a quasi-static elongation dl along the tetanus, the *external* force F must perform a work $Fdl = dW$. It is natural to identify the function $W(l)$ with the energy stored in the passive machinery inside an individual HS. Observe that the elongation dl may involve not only elastic deformation but also *structural* changes associated, for instance, with the variation in the number of the attached cross-bridges.

If we now apply this line of reasoning to the 'up–down–up' isometric tetanus curve $F(l)$ for a single HS we obtain a double-well energy function $W(l)$. By subtracting the quadratic contribution due to parallel linear elasticity we obtained the 'actively stored' energy function $W_a(l)$, which has the form of a Lennard–Jones potential. The convex section of this potential is associated with the 'ascending limb'. Here the energy grows with stretch because initially neutralized, non-force-bearing cross-bridges get recruited with an increased stretch (become 'force-bearing') and more of them contribute to the storage of elastic energy by pulling on the internal elastic springs. When the length of a HS increases beyond the inflection point of the tetanus curve (point of optimal overlap) the system enters the descending limb where progressive 'damage' starts to develop. The associated sequential de-bonding of cross-bridges diminishes the elastic contribution to the stored energy while increasing the contribution due to the surface/cohesion energy associated with de-bonded cross-bridges. After all bonds have been broken, the stored energy becomes fully cohesive and does not change any more while the generated force becomes equal to zero.

If we now consider a chain of HSs with the total length fixed we can argue that in view of the dissipative kinetics the system will select a mechanical configuration where the energy invested by pullers in the loading of passive sub-structures is locally *minimized*. On the descending limb this selection principle will then ensure an optimal *tradeoff* between elasticity and damage. Note that such an interpretation of the homeostasis in a muscle myofibril is in agreement with the conventional assumption that active contractile machinery inside a cell rearranges itself to minimize the elastic energy generated in the environment [72, 73].

If this interpretation is adopted, the problem of finding the energy minimum in isometric conditions can be formulated as follows

$$\bar{w}(\bar{\varepsilon}) = \min_{\{\varepsilon_i,\ \sum_{i=1}^{N}\varepsilon_i = N\bar{\varepsilon}\}} \frac{1}{N}\sum_{i=1}^{N} w(\varepsilon_i) \tag{3}$$

where

$$w(\varepsilon) = \begin{cases} \frac{1+E_0}{2}\varepsilon^2 & , \quad \varepsilon \le 1 \\ -\frac{E}{2}\left(\varepsilon - \frac{1+E}{E}\right)^2 + \frac{E_0}{2}\varepsilon^2 + \frac{1+E}{2E} & , \quad 1 < \varepsilon < \frac{1+E}{E} \\ \frac{E_0}{2}\varepsilon^2 + \frac{1+E}{2E} & , \quad \varepsilon \ge \frac{1+E}{E} \end{cases}. \tag{4}$$

is the dimensionless double-well stored energy characterizing a single HS. The system of equilibrium equations in this problem is exactly (1). To identify local minima of the energy we first rewrite the energy as a function of N–1 variables [66]

$$\hat{w}(\varepsilon_1, ..., \varepsilon_{N-1}) = N^{-1}\left[\sum_{i=1}^{N-1} w(\varepsilon_i) + w(N\bar{\varepsilon} - \sum_{i=1}^{N-1}\varepsilon_i)\right]. \tag{5}$$

The equilibrium configuration $\varepsilon_i(\bar{\varepsilon})$, $i=1,\ldots,N$–1 is a local minimum of the energy (5) if the Hessian matrix of the second derivatives

$$\left\|\frac{\partial^2 \hat{w}}{\partial\varepsilon_i \partial\varepsilon_j}\right\| = N^{-1}\begin{Vmatrix} \hat{E}_1 + \hat{E}_N & \hat{E}_N & \ldots & \hat{E}_N \\ \hat{E}_N & \hat{E}_2 + \hat{E}_N & \ldots & \hat{E}_N \\ \ldots & \ldots & \ldots & \ldots \\ \hat{E}_N & \hat{E}_N & \ldots & \hat{E}_{N-1} + \hat{E}_N \end{Vmatrix} \tag{6}$$

is positive definite. Here, $\hat{E}_i = w''(\varepsilon_i)$, $i=1,\ldots,N$ and ε_i represent a solution of the equilibrium equations. The necessary and sufficient conditions for the matrix (6) to be positive definite can be written in the form $A_j>0$, $j=1,\ldots,N$–1, where

$$A_j \equiv \left(\prod_{i=1}^{j}\hat{E}_i\right)\left(1 + \sum_{i=1}^{j}\frac{\hat{E}_N}{\hat{E}_i}\right) \tag{7}$$

are the principal minors of the matrix (6) , see [17]. Observe that if $l = 0$, all $\hat{E}_i>0$ and the matrix (6) is positive definite. In contrast, if $l \ge 2$ the configuration is unstable because one can always rearrange the springs to have $A_1 = \hat{E}_1 + \hat{E}_N \le 0$, see [16]. Finally, if $l = 1$, we can always assume that $\hat{E}_{N-1} < 0$. Then $A_i > 0$ for $i=1,\ldots, N$–2 and stability depends on the sign of A_{N-1}. According to (7)

$$A_{N-1} = (\hat{E}(\varepsilon_I))^{N-m-1}\hat{E}(\varepsilon_{II})(\hat{E}(\varepsilon_{III}))^m\left(\frac{N-m-1}{\hat{E}(\varepsilon_I)} + \frac{1}{\hat{E}(\varepsilon_{II})} + \frac{m}{\hat{E}(\varepsilon_{III})}\right)$$

and since $\hat{E}(\varepsilon_{II}) < 0$, the stability condition reads

$$\frac{N-m-1}{1+E_0} - \frac{1}{E-E_0} + \frac{m}{E_0} < 0. \tag{8}$$

This inequality has a simple geometrical interpretation: since the springs are connected in series the effective elastic modulus $E_* = \bar{f}'(\bar{\varepsilon})$ of the whole chain can be expressed as $E_*^{-1} = N^{-1}\sum_{i=1}^{N}\hat{E}_i^{-1}$ and then according to (8) configuration with $l = 1$ is stable if and only if $E_* < 0$ (see [66]).

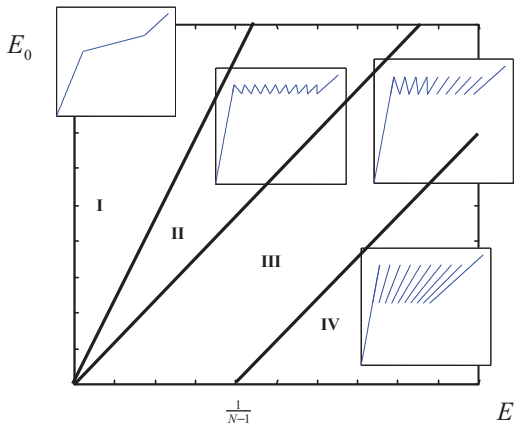

Figure 8. Phase diagram in the parameter space (E_0, E). Three lines divide the first quadrant into four regions of qualitatively different behavior: line $E_0 - E = 0$ separating regimes **I** and **II**; line $NE_0 - (N-1)E = 0$ separating regimes **II** and **III** and line $NE_0 - (N-1)E + 1 = 0$ separating regimes **III** and **IV**. The typical force–length curves (sets of metastable branches) in each of the four regimes are shown in the boxes.

By using (8) we can identify in the space (E_0,E) the areas with qualitatively deferent behavior, see Figure 8. For instance, if $E_0 \geq E$ the solution of the minimization problem (3) is trivial and the only equilibrium configurations are the homogeneous (affine) ones (region **I**). When $E_0 < E < \frac{N}{N-1}E_0$ all equilibrium branches with $l = 1$ are stable and solution remains unique even though the HS length distribution is no longer affine (region **II**). As E is increased at constant E_0, branches with $l=1$ become progressively unstable and the number of local minima corresponding to nonaffine configurations increases (region **III**). At $E \geq E_0\frac{N}{N-1} + \frac{1}{N-1}$ (region **IV**) all configurations containing HSs in phase *II* are unstable and the energy landscape exhibits the richest variety of local minima. One can say that in the domain $E \geq \frac{N}{N-1}E_0$ the energy surface is rugged and the hysteretic (memory) behavior can be expected. Note that for sufficiently large N any myofibril with $E_0 < E$ is in region **IV** and the typical configuration around the descending limb is nonaffine.

To find the global minimum of the energy we need to compare the energies of all metastable branches at a given $\bar{\varepsilon}$. Based on the analysis of the local stability, we can reduce the class of competitors to just two major groups $(N-m, 0, m)$ and $(N-m\text{-}1, 1, m)$. First, consider the case when all configurations with $l = 1$ are unstable (region **IV**). In order to find the global minimum of the energy one needs to choose among the configurations $(N-m, 0, m)$ with the equilibrium energies

$$\bar{w}(\bar{\varepsilon}, m) = \frac{1+E_0}{2\left(1+\frac{m}{NE_0}\right)}\bar{\varepsilon}^2 + \frac{(E+1)m}{2EN}. \tag{9}$$

These branches are defined in the domains $[\bar{\varepsilon}_{m^*}, \bar{\varepsilon}^*_m]$, where

$$\bar{\varepsilon}_{m^*} = \frac{E_0(E+1)}{E(E_0+1)}\left(1+\frac{m}{NE_0}\right), \bar{\varepsilon}^*_m = 1+\frac{m}{NE_0}.$$

Introduce the points of intersection of the metastable branch $\bar{w}(\bar{\varepsilon}, m)$ with the branches $\bar{w}(\bar{\varepsilon}, m-1)$ and $\bar{w}(\bar{\varepsilon}, m+1)$

$$\bar{\varepsilon}^{\pm}_m = \sqrt{\frac{E_0(E+1)}{E(E_0+1)}\left(1+\frac{m\pm 1}{NE_0}\right)\left(1+\frac{m}{NE_0}\right)}.$$

It is then straightforward to check that for $\bar{\varepsilon} \in [\bar{\varepsilon}^-_m, \bar{\varepsilon}^+_m] \subset [\bar{\varepsilon}_{m^*}, \bar{\varepsilon}^*_m]$ we have $\bar{w}(\bar{\varepsilon}, m) < \bar{w}(\bar{\varepsilon}, \tilde{m})$, for any $\tilde{m} \neq m$, meaning that configuration $(N-m, 0, m)$ is the global minimizer in this interval.

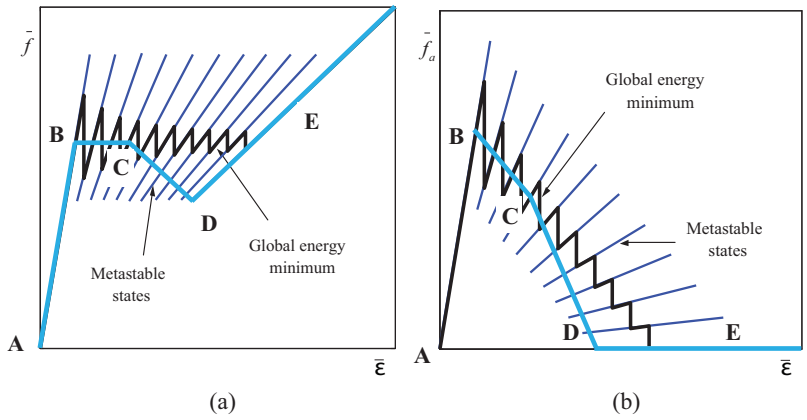

Figure 9. Anticipated structure of the isometric force–length relation for a tetanized muscle fiber superimposed on the full set of all metastable branches. Global minimizers and metastable states are illustrated for the chain with $N = 10$: (a) the total force and (b) the active force. Absolute minima are shown by bold lines, metastable states by solid lines. Blue thick line (color on line) shows the proposed interpretation of the isometric tetanus curve.

Next consider regions **II** and **III** containing metastable configurations with $l = 1$. Note that each branch $(N - m - 1, 1, m)$ connects the end points $\bar{\varepsilon}^*_m$ and $\bar{\varepsilon}_{m+1^*}$ of the branches $(N - m, 0, m)$ and $(N - m - 1, 0, m + 1)$. In the case when $\bar{\varepsilon}^*_m < \bar{\varepsilon}_{m+1^*}$ (our Equation (8)), the configuration $(N - m - 1, 1, m)$ is the only local minimizer in the interval $[\bar{\varepsilon}^*_m, \bar{\varepsilon}_{m+1^*}]$. Outside these intervals all configurations with $l = 1$ are unstable and the global minimum of the energy is achieved at the configurations $(N - m, 0, m)$.

In the continuum limit $N \to \infty$ the global minimum of the energy can be selected among the pieces of parabolas $\bar{w}(\bar{\varepsilon}, m)$ given by (9) and we need to compute $\bar{w}(\bar{\varepsilon}) = \inf_{z \in [0,1]} \bar{w}(\bar{\varepsilon}, z)$. If configuration is nonaffine and $0 < z < 1$ we obtain

$$\bar{w}(\bar{\varepsilon}) = \bar{\varepsilon}\sqrt{\frac{E_0(1+E_0)(1+E)}{E}} - \frac{E_0(1+E)}{2E}.$$

This relation describes a straight line in the energy–strain plane furnishing a *convexification* of the original nonconvex energy function $w(\bar{\varepsilon})$. The (Maxwell) force describing the 'coexistence' of long and short HSs is then

$$\bar{w}'(\bar{\varepsilon}) = \bar{f}(\bar{\varepsilon}) = \sqrt{\frac{E_0(1+E_0)(1+E)}{E}}.$$

2.4. An interpretation of the isometric tetanus

We are now in the position to propose an interpretation of the observed *macroscopic* force–length relation for an isometrically activated myofibril (tetanus curve).

First of all we observe that the *global* energy minimization scenario contradicts observations because the negative overall stiffness is incompatible with the convexification of the energy. Moreover, the global minimization scenario predicts considerable amount of vastly over-stretched (popped) HSs that have not been seen in experiments. We are then left with a conclusion that along the isometric tetanus at least some of the active non-affine configurations correspond to *local* rather than global minimum of the stored energy. A realistic interpretation of the experimentally observed tetanus curve as a combination of local and global minimization segments is presented in Figure 9.

In view of the quasi-elastic nature of the corresponding response, it is natural to associate the ascending limb of the tetanus curve at small levels of stretch with the homogeneous (affine) branch of the global minimum path (segment AB in Figure 9). Around the point where the global minimum configuration first starts being nonaffine (point B in Figure 9), it is conceivable that a constitutive trajectory remains close to the global minimum path. Then, the isometric tetanus curve forms a plateau separating

ascending and descending limbs (segment between points B and C in Figure 9). Such plateau is indeed observed in experiments on myofibrils and is known to play an important physiological role ensuring robustness of the active response. We can speculate that a limited mixing of 'strong' and 'weak' (popped) HSs responsible for this plateau is confined close to the ends of a myofibril while remaining almost invisible in the bulk of the sample.

To account for the descending limb, we must assume that as the length of the *average* HS increases beyond the end of the plateau (point C in Figure 9), the tetanized myofibril fails to reach the global minimum of the stored energy. To match observations we assume that beyond point C in Figure 9 the attainable metastable configurations are characterized by the value of the active force, which deviates from the Maxwell value and becomes progressively closer to the value generated by the homogeneous configurations as we approach the state of no overlap (point D). We have seen that the corresponding nonaffine configurations can be reached dynamically as a result of the instability of a homogeneous state. One can speculate that such almost affine metastable configurations may be favored due to the presence of some additional mechanical signaling loops which take a form of inter-sarcomere stiffness [63] or next to nearest neighbor interaction [74, 75]. As the point D in Figure 9 is reached, all cross-bridges are detached and beyond this point the myofibril is supported exclusively by the passive parallel elastic elements (segment DE).

Note next that since all of the metastable nonaffine states involved in this construction have an extended range of stability, the application of a sudden deformation will take the system away from the so-defined isometric tetanus curve (curve BCD in Figure 9). It is then difficult to imagine that the isometric relaxation following such an eccentric loading will allow the system to stabilize again exactly on the curve BCD. The response predicted by this model is therefore consistent with the fact that the residual force enhancement was observed not only around the descending limb but also above the optimal (physiological) plateau and even around the upper end of the ascending limb [76, 77]. It is also consistent with the observations showing that the residual force enhancement after stretch is independent of the velocity of the stretch, that it increases with the amplitude of the stretch and that it is most pronounced along the descending limb. In summary, the model can serve as a plausible explanation of the hysteresis and history-dependent response observed in tetanized muscles. It suggests that trapping in the local minima of the stored energy is a probable origin of the multi-validness of the tension–length relation.

One of the main conclusions of this analysis is that the nonuniqueness of the muscle response around the descending limb is not a property of an individual HS but rather a collective property of the whole myofibril. More specifically, a comparison of the force–length relation ABCDE in Figure 9 with the force–length relation for a single HS suggests that the collective tetanus may be rather different from the tetanus of an individual HS. The origin of this difference is the nonaffine nature of the response of the myofibril which complicates the interpretation of the macroscopic force–length relations in terms of the behavior of the elementary units: indeed, during collective relaxation of a multi-sarcomere system the dynamic lengths of individual HSs can be neither controlled nor monitored [78]. Ultimately, the nonaffine (non-Cauchy–Born) character of the deformation of the 'muscle material', presenting itself as a HS inhomogeneity, is a consequence of the nonconvexity of the stored energy and an outcome of an *optimization* between the cost of stretching and the cost of damage.

3. A nonlocal extension of the model

The analysis presented in Section 2 reveals considerable degeneracy of the local model since all strain configurations related by permutations are equivalent. In particular, the local model cannot distinguish among energetically equivalent nonaffine arrangements of 'strong' and 'weak' HSs. In this section, we attempt to limit the degeneracy by introducing the long-range mechanical signaling between individual HSs. The implied mechanical interactions mimic the presence of connecting/supportive tissues that prevent the break up of the meshwork of myofilaments and keep the HSs in a relative register across the myofibril.

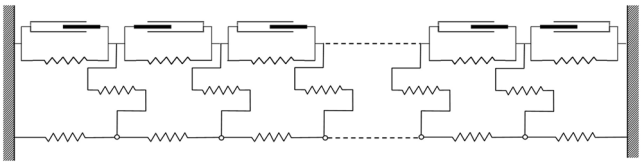

Figure 10. Schematic representation of the HS chain surrounded by connecting tissue.

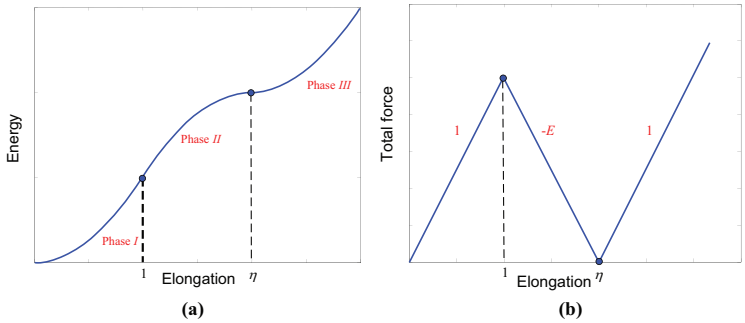

Figure 11. The dimensionless energy–length (a) and the force–length (b) relations describing an individual contractile unit in the nonlocal model.

3.1. The mechanism of long-range interactions

Consider two parallel elastically coupled chains shown in Figure 10. One of the chains, composed of softening contractile elements describing individual HSs, is exactly the same as in the local model presented in Section 2. The other chain contains linear springs mimicking additional elastic interactions in the myofibril of possibly non-one-dimensional nature. We assume that the coupling, provided by shear (leaf) springs is linearly elastic. In dimensionless form the stored energy of the resulting mechanical system reads

$$\bar{w}(\bar{\varepsilon}, \mathbf{u}, \mathbf{v}, N) = N^{-1} \sum_{i=1}^{N} w(u_i - u_{i-1}) + \frac{1}{2} E_{\perp} (u_i - v_i)^2 + \frac{1}{2} E_{||} (v_i - v_{i-1})^2. \tag{10}$$

Here u_i is the displacement of the ith node of the HS chain and v_i is the displacement of the ith node in the elastic background. The two new dimensionless parameters $E_{\perp}$ and $E_{||}$ characterize the shear and the Young moduli of the background. We choose the double-well potential $W(\varepsilon)$ describing the energy of a single HS in the form (see Figure 11)

$$w(x) = \begin{cases} \dfrac{1}{2} x^2 & , \quad \varepsilon \leq 1 \\ -\dfrac{(x-\eta)^2}{2(\eta - 1)} + \dfrac{\eta}{2} & , \quad 1 < \varepsilon < \eta \\ \frac{1}{2}(x-\eta)^2 + \dfrac{\eta}{2} & , \quad \varepsilon \geq \eta \end{cases} \cdot \tag{11}$$

This potential is qualitatively similar to that used in Section 2, in particular, the active contribution is exactly the same as before. The passive force is assumed to be negligible until there is no more overlap between the actin and myosin filaments and to be linear afterwards: this description of the passive element is more realistic than that given in Section 2. The assumption that phases *I* and *III* have the same elastic moduli is made for convenience since it considerably simplifies analytical computations.

Note that the nonlocal model described by the energy (11) involves *competing interactions*: the double-well potential favors sharp boundaries between the 'phases' while the elastic foundation term

favors strain uniformity. As a result of this competition the energy minimizing system is expected to find an optimal tradeoff between the uniformity at the macro-scale and the nonuniformity (nonaffinity) at the micro-scale.

Suppose now that the myofibril described by the energy (11) is loaded in a hard device so that $u_0 = v_0 = 0$ and $u_N = v_N = N\bar{\varepsilon}$. Then the equilibrium problem reduces to finding

$$\bar{w}(\bar{\varepsilon}, N) = \min_{\substack{\{u_i, v_i, u_0 = v_0 = 0, \\ u_N = v_N = N\bar{\varepsilon}\}}} \bar{w}(\bar{\varepsilon}, \mathbf{u}, \mathbf{v}, N). \tag{12}$$

The corresponding system of equilibrium equations

$$\begin{aligned} &w'(u_i - u_{i-1}) - w'(u_{i+1} - u_i) + E_\perp(u_i - v_i) = 0\,, \\ &E_{||}(2v_i - v_{i+1} - v_{i-1}) + E_\perp(v_i - u_i) = 0, \end{aligned}$$

is highly nonlinear and can be expected to have multiple solution.

3.2. Elimination of linear elastic degrees of freedom

To make an analytical study of this nonlinear system possible we neglect the presence of the spinodal region (phase *II*) which played only a minor role in Section 2 and consider a bi-quadratic representation of our two energy wells: $w(x) = w_0(x) + Sw_1(x)$, where $w_0(x) = \frac{1}{2}x^2 - \alpha x + \beta; w_1(x) = -\alpha x + \beta$, $\alpha = \frac{\eta}{2}$, $\beta = \frac{\eta^2 + \eta}{4}$ and S is a spin variable distinguishing phases *I* and *III*

$$S = \begin{cases} -1 & for \quad phase\ I \\ 1 & for \quad phase\ III. \end{cases}$$

Now any micro-configuration can be specified by the vector $\mathbf{S} = \|S_1, S_2, ..., S_N\|$, in particular, the fraction of HS in phase *III* is

$$\omega = \frac{1}{N}\sum_{i=1}^{N}\frac{S_i + 1}{2}. \tag{13}$$

For this type of configurations the energy (10) can be rewritten as

$$\bar{w}(\bar{\varepsilon}, \mathbf{u}, \mathbf{v}, \mathbf{S}, N) = N^{-1}\sum_{i=1}^{N} w_0(u_i - u_{i-1}) + S_i w_1(u_i - u_{i-1}) + \frac{1}{2}E_\perp(u_i - v_i)^2 + \frac{1}{2}E_{||}(v_i - v_{i-1})^2. \tag{14}$$

By minimizing out in this expression the linear variables u_i, v_i at a given $\mathbf{S}$, which involves an inversion of a tri-diagonal matrix, we obtain

$$\begin{aligned} u_i &= i\bar{\varepsilon} - \frac{\eta E_\perp \sinh(i\theta)}{\sinh\theta \sinh(N\theta)}\sum_{j=1}^{N-1}\mu_j \sinh(N-j)\theta + \frac{\eta E_\perp}{\sinh\theta}\sum_{j=1}^{i-1}\mu_j \sinh(i-j)\theta + \eta\mu_i \\ v_i &= i\bar{\varepsilon} + \frac{\eta E_\perp \sinh(i\theta)}{E_{||}\sinh\theta \sinh(N\theta)}\sum_{j=1}^{N-1}\mu_j \sinh(N-j)\theta - \frac{\eta E_\perp}{E_{||}\sinh\theta}\sum_{j=1}^{i-1}\mu_j \sinh(i-j)\theta \end{aligned} \tag{15}$$

where

$$\theta = 2\sinh^{-1}\left(0.5\sqrt{\frac{E_\perp(1 + E_{||})}{E_{||}}}\right), m_i = \sum_{j=1}^{i}\frac{S_j + 1}{2}, \mu_i = m_i - i\omega.$$

Note that m_i is the number of HSs in phase *III* located between the first and the ith node. By substituting (15) into (14) and omitting the 'boundary' terms of the order $1/N$, we obtain the expression for the energy in terms of the components of vector $\mathbf{m}$

$$\bar{w}(\bar{\varepsilon}, \mathbf{m}, N) = w_0(\bar{\varepsilon}) + \frac{1}{2}E_{||}\bar{\varepsilon}^2 + w_1(\bar{\varepsilon})(2\omega - 1) + \frac{\eta^2\omega}{2}\left(\frac{\omega}{1+E_{||}} - 1\right) + \frac{1}{N}\sum_{i=1}^{N-1}\sum_{j=1}^{N-1} K(|i-j|)(m_i - m_j)^2 \quad (16)$$

where

$$K(n) = \eta^2 E_{\perp}\frac{\cosh\theta - 1}{4\sinh\theta}e^{-n\theta} > 0.$$

One can show that for any $\{u_i, v_i\}$ the second variation of the energy (14) is positive definite and therefore all equilibrium states with a prescribed configuration $\mathbf{m}$ are metastable. The corresponding equilibrium force–length relations can be written in the form

$$f(\bar{\varepsilon}, \mathbf{m}, N) = \frac{d\bar{w}(\bar{\varepsilon}, \mathbf{m}, N)}{d\bar{\varepsilon}} = (1 + E_{||})\bar{\varepsilon} - \eta\omega. \quad (17)$$

In Figure 12 we illustrate the relations (17) for the case $N = 51$. The energies of the corresponding metastable branches are presented in Figure 13 where we show two different scales illustrating the emerging self-similarity.

3.3. The global minimum of the energy

To reconstruct the global minimum of the energy we need to compare the energies $\bar{w}(\bar{\varepsilon}, \mathbf{m}, N)$ for different 'configurations' $\mathbf{m}$. Due to the special structure of the function $\bar{w}(\bar{\varepsilon}, \mathbf{m}, N)$ it is natural to first fix the fraction ω of the HS in phase *III*, and search for configurations $\mathbf{m}$, delivering the global minimum to the energy

$$\bar{w}(\bar{\varepsilon}, \omega, N) = \min_{\{\mathbf{m},\, m_N = N\omega\}} \bar{w}(\bar{\varepsilon}, \mathbf{m}, N)$$

It turns out that the energy (16) has the same overall structure as the equilibrium energy of a harmonic chain of atoms adsorbed on a periodic piecewise parabolic potential with an incommensurate reference length scale [79]. This problem was solved in [67] and we just need to accommodate their result for our case.

First of all, based on a theorem proved in [67] we can claim that the configuration with the minimal energy is precisely

$$m_i = [i\omega], \quad (18)$$

where $[x]$ is the integer part of x. In terms of the 'spin' variables the minimum energy configuration can be written as

$$S_i = 2[i\omega] - 2[(i-1)\omega] - 1. \quad (19)$$

One can see that the microscopic state is periodically modulated, guaranteeing the finest possible mixture of phases, and thus providing the macroscopically homogeneous deformation. This is consistent with muscle experiments where only a small extent of regional non uniformities was observed in the (averaging) laser diffraction studies [40, 80] and where over-lengthened HS were found to be 'scattered' [34].

3.4. The continuum limit

By substituting (18) into (16), we can obtain an expression of the energy in terms of ω for any N, however, we can fully analyze the result only in the thermodynamic (continuum) limit and therefore in what

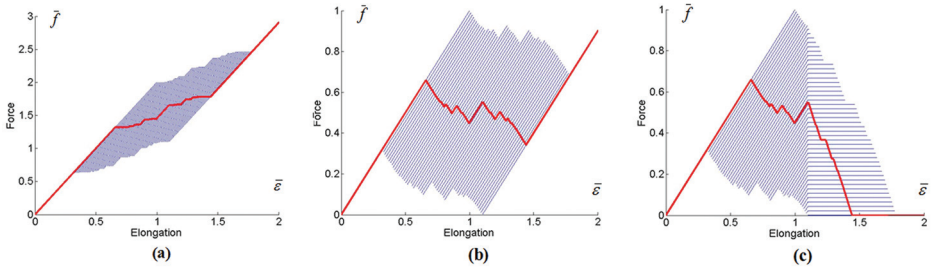

Figure 12. Metastable force–length branches for the nonlocal model with $N = 51$, $E = 10$, $E_{\perp} = 1$, $E_{||} = 1$: (a) total force, (b) total force with subtracted contribution due to connecting tissue, (c) total force with subtracted contributions due to connecting tissue and due to parallel passive elasticity. The force–length relation along the global energy minimum (Maxwell) path in the continuum limit ($N = \infty$) is shown in red.

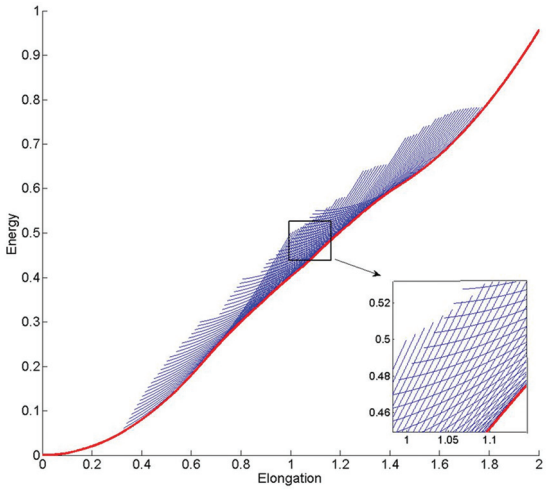

Figure 13. Metastable energy-length branches for a nonlocal chain with the contribution due to connecting tissue subtracted. Here, $N = 51$, $E = 10$, $E_{\perp} = 1$, $E_{||} = 1$. Two different scales illustrate the developing self-similar pattern. The global energy minimum in the continuum limit ($N = \infty$) is shown in red.

follows we only deal with the limit $\bar{w}(\bar{\varepsilon}, \omega) = \lim_{N\to\infty} \bar{w}(\bar{\varepsilon}, \omega, N)$. The limiting energy can be represented in the form of an infinite series

$$\bar{w}(\bar{\varepsilon}, \omega) = w_0(\bar{\varepsilon}) + \tfrac{1}{2}E_{||}\bar{\varepsilon}^2 + w_1(\bar{\varepsilon})(2\omega - 1) + \frac{\eta^2\omega}{2}\left(\frac{\omega}{1+E_{||}} - 1\right) + \psi(\omega), \tag{20}$$

$$\psi(\omega) = 2\sum_{n=1}^{\infty} K(n)\Big(n\omega(2[n\omega] + 1) - [n\omega]^2 - [n\omega]\Big).$$

Observe that if $n\omega$ is not an integer (if ω is irrational) the function $\bar{w}(\bar{\varepsilon}, \omega)$ is differentiable with respect to ω. The derivative, however, does not exist when $n\omega$ is an integer, i.e. whenever ω is rational. Therefore, if we define $\omega_{\bar{\varepsilon}}$ by the implicit formula

$$\bar{w}(\bar{\varepsilon}, \omega_{\bar{\varepsilon}}) = \inf_{\omega\in[0,1]} \bar{w}(\bar{\varepsilon}, \omega),$$

we can have two options:

(a) the inf is attained at a point of differentiability, i.e. there exists an irrational ω_{ir} such that $\frac{\partial\bar{w}(\bar{\varepsilon}, \omega)}{\partial\omega} = 0$. In this case ω_{ir} is a root of an equation

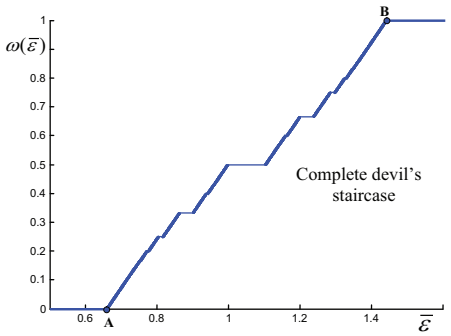

Figure 14. The fraction of the HSs in phase *III* as a function of the average strain $\bar{\varepsilon}$ in the nonlocal model (E = 10, $E_\perp$ = 1, $E_{||}$ = 1, $N = \infty$).

$$\bar{\varepsilon} = \frac{2}{\eta}\sum_{n=1}^{\infty} nK(n)(2[n\omega_{ir}]+1) + \frac{\eta+1}{2} + \frac{\eta}{2}\left(\frac{2\omega_{ir}}{1+E_{||}} - 1\right); \tag{21}$$

(b) the inf is attained at a point ω where the derivative experiences a discontinuity. This means that there exists a rational point, ω_r, such that $\frac{\partial \bar{w}(\bar{\varepsilon},\omega)}{\partial \omega}\Big|_{\omega=\omega_r-0} \leq 0$ and $\frac{\partial \bar{w}(\bar{\varepsilon},\omega)}{\partial \omega}\Big|_{\omega=\omega_r+0} \geq 0$.

In fact, following [67] one can show that the minimizer $\omega(\bar{\varepsilon})$ in our problem has a form of a complete devil's staircase: an increasing continuous function which is flat outside a countable number of points. More precisely, we observe that each rational value $\omega_r = \frac{r}{s}$, where r and s are irreducible integers, is a minimizer in a finite interval $(\bar{\varepsilon}_{r/s-}, \bar{\varepsilon}_{r/s+})$ where

$$\begin{aligned} \bar{\varepsilon}_{r/s+} &= \frac{2}{\eta}\sum_{n=1}^{\infty} nK(n)\left(2\left[\frac{nr}{s}\right]+1\right) + \frac{\eta+1}{2} + \frac{\eta}{2}\left(\frac{2r}{s(1+E_{||})} - 1\right), \\ \bar{\varepsilon}_{r/s-} &= \frac{2}{\eta}\sum_{n=1}^{\infty} nK(n)\left(2\left[\frac{nr}{s}\right]^{-}+1\right) + \frac{\eta+1}{2} + \frac{\eta}{2}\left(\frac{2r}{s(1+E_{||})} - 1\right). \end{aligned} \tag{22}$$

Here by $[x]^-$ we denote the largest integer smaller than x. The width of these steps can be given explicitly

$$\Delta\bar{\varepsilon}\left(\frac{r}{s}\right) = \frac{\eta E_\perp(\cosh\theta - 1)}{2\sinh\theta(\cosh(s\theta) - 1)}.$$

The resulting deformation is non-affine ($0 < \omega < 1$) in the interval $(\bar{\varepsilon}(0), \bar{\varepsilon}(1))$, where

$$\bar{\varepsilon}(0) = \lim_{\omega\to 0+}\bar{\varepsilon}_\omega = \frac{\eta E_\perp}{4\sinh\theta} + \frac{1}{2}, \bar{\varepsilon}(1) = \lim_{\omega\to 1-}\bar{\varepsilon}_\omega = -\frac{\eta E_\perp}{4\sinh\theta} + \frac{\eta E_\perp}{2(\cosh\theta - 1)} + \frac{1}{2} + \frac{\eta}{E_{||}+1}.$$

The structure of the function $\omega_{\bar{\varepsilon}} = \omega(\bar{\varepsilon})$ defined by (21)–(22) is illustrated in Figure 14. The 'staircase' character of this function suggests that the predictions of the model are *robust* in the sense that a particular microstructure corresponds to a finite domain in the space of parameters. To illustrate this point further we show in Figure 15 the phase diagram where parameters are the strength of the elastic coupling and the applied stretch. This diagram has a typical 'tongue' structure characterizing systems with incommensurate competing interactions, see [67].

3.5. Force–length relation

By substituting the minimizer $\omega_{\bar{\varepsilon}} = \omega(\bar{\varepsilon})$ into the energy function (20) we obtain the relaxed energy function describing the myofibril whose (nonaffine) internal configurations are the globally minimizers:

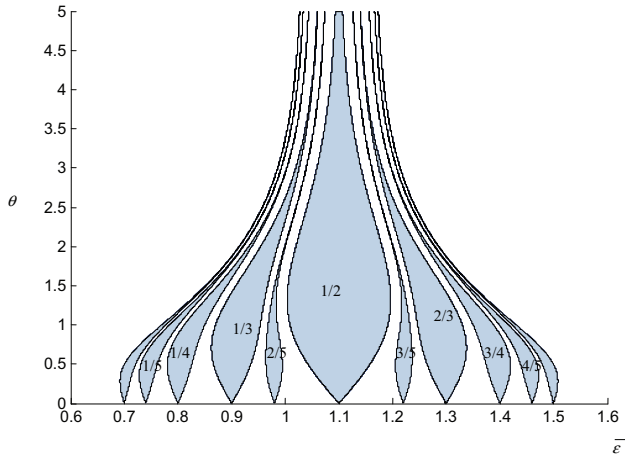

Figure 15. The θ–$\bar{\varepsilon}$ phase diagram: shaded areas correspond to periodic (commensurate) ground states; the number inside each shaded area gives the fraction of HSs in phase *III*. Parameters: $E = 5$, $E_{||} = 5$, $N = \infty$.

$$\bar{w}(\bar{\varepsilon}) = \begin{cases} \dfrac{1+E_{||}}{2}\bar{\varepsilon}^2; & \bar{\varepsilon} \in (0, \bar{\varepsilon}(0)) \\ \dfrac{1+E_{||}}{2}\bar{\varepsilon}^2 - \bar{\varepsilon}\dfrac{\eta r}{s} + \psi\left(\dfrac{r}{s}\right) + \dfrac{\eta r}{2s} + \dfrac{\eta^2 r^2}{2s^2(1+E_{||})}; & \bar{\varepsilon} \in (\bar{\varepsilon}_{r/s-}, \bar{\varepsilon}_{r/s+}) \\ \dfrac{1}{2}(\bar{\varepsilon}-\eta)^2 + \dfrac{1}{2}E_{||}\bar{\varepsilon}^2 + \dfrac{\eta}{2}; & \bar{\varepsilon} \in (\bar{\varepsilon}(1), \infty) \end{cases} \tag{23}$$

The structure of the function $\bar{w}(\bar{\varepsilon})$ is illustrated in Figure 16 where the bold (red) line, represents global minimizers, while the solid (blue) line shows the energy of affine deformations. The nonaffine HS patterns minimizing the energy are detailed in Figure 17.

Finally, we write the overall force–length relation along the global minimum (Maxwell) path

$$f(\bar{\varepsilon}) = \bar{w}'(\bar{\varepsilon}) = \begin{cases} (1+E_{||})\bar{\varepsilon}; & \bar{\varepsilon} \in (0, \bar{\varepsilon}(0)) \\ (1+E_{||})\bar{\varepsilon} - \dfrac{\eta r}{s}; & \bar{\varepsilon} \in (\bar{\varepsilon}_{r/s-}, \bar{\varepsilon}_{r/s+}) \\ (1+E_{||})\bar{\varepsilon} - \eta; & \bar{\varepsilon} \in (\bar{\varepsilon}(1), \infty) \end{cases} \tag{24}$$

The function $f(\bar{\varepsilon})$ is illustrated in Figure 18(a). One can see that the plateau, characterizing the energy minimizing states in the local model, is now replaced by a curve with a positive slope. The fact that the overall elastic modulus is now positive reflects the presence of the connecting tissue that is stressed whenever the myofibril is in a nonaffine state.

If we now subtract the contribution due to the connecting tissues and therefore focus on the mechanical behavior of the 'naked' myofibril, we obtain the force length relation shown in Figure 18(b). Note that this curve has an overall negative slope even though at each point the instantaneous elastic modulus is strictly positive. The negative overall slope is even more pronounced in Figure 18(c) where all passive elasticity has been subtracted.

To summarize, the nonlocal extension of the chain model lacks the permutation degeneracy and generates specific microstructures with fine mixing of shorter HSs located on the ascending limb of the tension–length curve and longer HSs supported mostly by the passive structures. The mixed configurations represent periodically modulated patterns that are undistinguishable from the homogeneous deformation if viewed at a coarse scale. The descending limb can be again interpreted as a union of positively sloped steps that can be now of vastly different sizes. It is interesting that the discrete structure of the

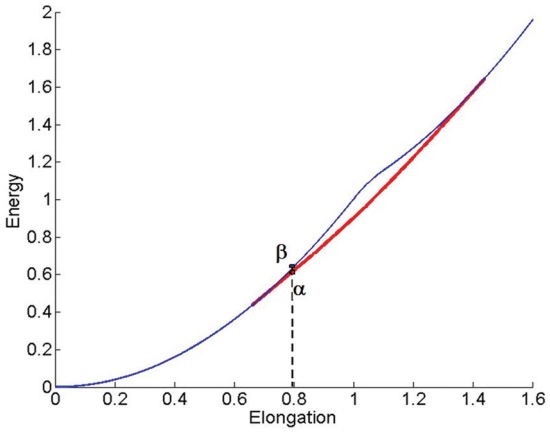

Figure 16. The global minimum of the energy in the continuum limit (bold line, state α), compared with the energy of the affine states (solid line, state β). Here $E = 10$, $E_{\perp} = 1$, $E_{||} = 1$, $N = \infty$.

force–length curve survives in the continuum limit, which instead of smoothening the constitutive relation makes it extremely singular.

To make the nonlocal model compatible with observations, we should follow the approach of Section 2, abandon the global minimum path and associate the descending limb with metastable (rather than globally stable) states. More specifically, we should apply an auxiliary construction similar to the one shown in Figure 9 for the local model, which anticipates an outcome produced by the realistic kinetic model of tetanization. A detailed implementation of these ideas for the nonlocal model supported by the numerical experiments based on a particular dynamic extension of the model will be presented elsewhere.

4. Conclusions

The goal of this paper is to contribute to the ongoing discussion whether the well-documented nonuniqueness of the mechanical response of skeletal muscles around the descending limb is a feature of an *individual* HS or a *collective* property of the whole myofibril.

To this end we developed a purely mechanical model of a tetanized muscle fiber amenable to a rather complete and transparent mathematical analysis. Following some previous work, we interpreted individual contractile elements (maximally tetanized HSs) as nonlinear elastic springs whose tension can decrease with length and modeled additional passive elements by parallel (nonlinear) elastic springs. To distinguish between multiple equilibrium states we introduced an energetic interpretation of equilibrium. Even though viewing mechanical equilibration, as *energy minimization* is rather unusual from the biological perspective we provided a justification for this approach in the context of tetanized muscles. We have shown that the energy can be understood as a mechanical work invested by the active pullers in elastic and inelastic deformation of the passive components of the force-generating machinery. We have also provided evidence that local minimization of such energy is compatible with the conventional dynamic extensions of the equilibrium model.

Our analysis of the local version of the proposed model convincingly demonstrated that the energy landscape of a myofibril is *rugged* and that the typical equilibrium configuration around the descending limb of the tension–length curve is *nonaffine*. Our model also suggests that around the descending limb the behavior of a chain of HSs differs considerably from a behavior of a single HS. We demonstrated that the complexity of the ensuing energy landscape explains the history-dependent mechanical response of tetanized muscles and clarifies the origin of stability of myofibrils on the descending limb. In particular, according to the model the overall *negative slope* of the tension–length curve on the descending limb should be viewed as a combination of a large number of abrupt steps with *positive slopes*.

The coexistence of a negative averaged (apparent) stiffness with the positive instantaneous stiffness is the main factor behind the mechanical stability of a myofibril on the descending limb. While along the

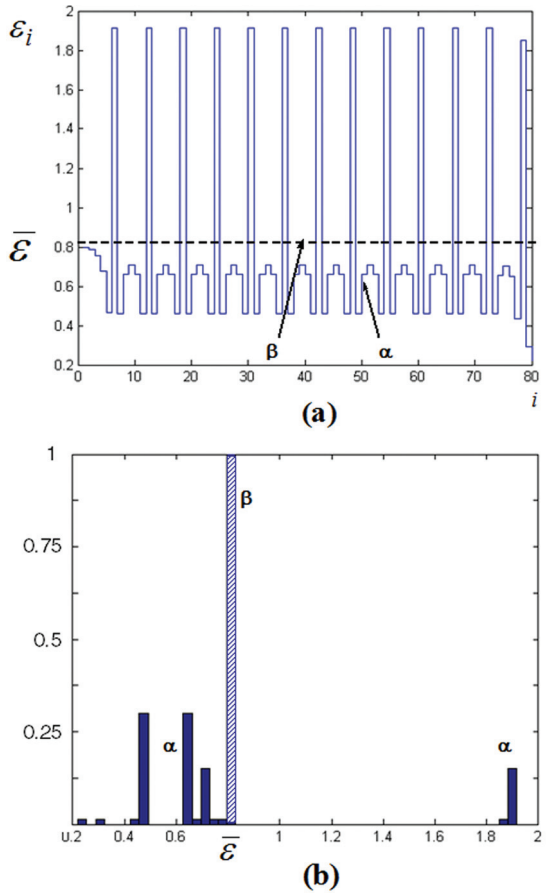

Figure 17. (a) The strain field corresponding to the global minimum of the energy at point α in Figure 16. The dashed line represents the strain of the affine deformation corresponding to point β in Figure 16. (b) Probability distribution function describing the fraction of HS with different strains. Parameters: $E = 3$, $E_{\perp} = 1$, $E_{||} = 100$, $\overline{\varepsilon} = 0.81$, $N = 80$.

Maxwell path most of the steps with a positive stiffness are very small, each one of them can be extended as a metastable branch. This interpretation is compatible with the hysteretic eccentric response of tetanized muscles suggesting that in the areas adjacent to both, the physiological plateau and the descending limb the muscle operates in an extended *domain of metastability*. The underlying complexity of the energy landscape fiber explains the observed dependence of the isometric tension on the pathway through which the elongation is reached.

To eliminate the permutational degeneracy associated with the local formulation of the chain model we proposed its nonlocal generalization that takes into account long-range interactions. On the descending limb the nonlocal model favors regular nonaffine configurations with a particular size distribution of HSs. More specifically, the mixed states exhibit fine periodically modulated patterns that are hardly distinguishable from the homogeneous deformation on the macro-scale. The energetically optimal variation of the degree of nonuniformity with stretch, predicted by the nonlocal model, exhibits a complete *devil's staircase*-type behavior. We emphasize, however, that in view of the over-damped nature of dynamics the corresponding low-energy micro inhomogeneous states may not be reachable even if the fiber is allowed to evolve through a sufficiently long creep phase.

The proposed equilibrium model does not address the question of equilibrium and non-equilibrium fluctuations that can push the system to explore much wider domains of the energy landscape. The model is also over simplistic in its representation of the parallel elastic elements that may exhibit complex unfolding patterns [81] as well as 'activity' of their own explaining experimentally observed stretch

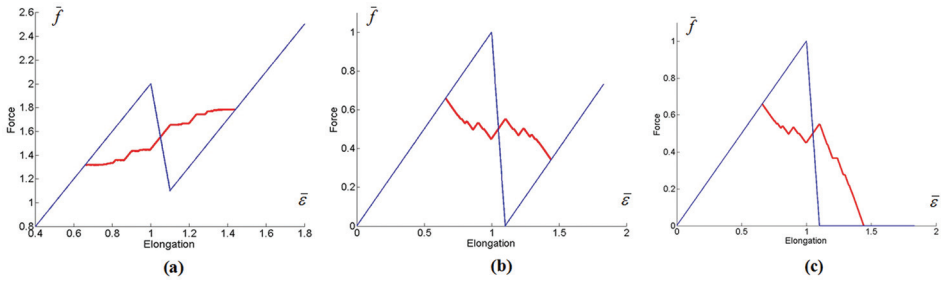

Figure 18. (a) The force–length relation in the nonlocal model along the global energy minimum path (continuum limit). (b) The same force–length relation with the contribution due to connecting tissue subtracted. (c) The same force–length relation with the contributions due to connecting tissue and due to HS passive elasticity subtracted. Here $E = 10$, $E_{\perp} = 1$, $E_{||} = 1$, $N = \infty$.

induced 'enhancement' of the passive force [82]. Our ability to simulate the mechanical behavior of muscles at this level of detail will open the way to direct comparison with experiments.

Acknowledgements

The authors appreciate stimulating discussions with M. Epstein and W. Herzog who initiated their interest in the subject of muscle mechanics and thank anonymous reviewers for their helpful comments.

Funding

This work is largely based on the PhD Thesis of IN defended in 2002 at the Department of Aerospace Engineering and Mechanics, University of Minnesota. LT is grateful for the NSF grants DMS-9803572 and DMS-010284 which supported this PhD project.

References

[1] McMahon, TA. *Muscles, reflexes, and locomotion*. Princeton, NJ: Princeton University Press; 1984.
[2] Woledge, RC, Curtin, NA, and Homsher, E. *Energetic aspects of muscle contraction*. London: Academic Press; 1985.
[3] Epstein, M, and Herzog, W. *Theoretical models of skeletal muscle: biological and mathematical considerations*. New York: Wiley, 1998.
[4] Howard, J. *Mechanics of motor proteins and the cytoskeleton*. Sunderland, MA: Sinauer Associates, 2001.
[5] Herzog, W, Leonard, TR, Joumaa, V, and Mehta, A. Mysteries of muscle contraction. *J Appl Biomech* 2008; 24(1): 1-13.
[6] Alberts, B. *Molecular biology of the cell*. 5th ed.New York: Garland Science, 2008.
[7] Gordon, AM, Huxley, AF, and Julian, FJ. The variation in isometric tension with sarcomere length in vertebrate muscle fibres. *J Physiol* 1966; 184(1): 170-192.
[8] ter Keurs, HE, Iwazumi, T, and Pollack, GH. The sarcomere length-tension relation in skeletal muscle. *J Gen Physiol* 1978; 72(4): 565-592.
[9] Julian, FJ, and Morgan, DL. The effect on tension of non-uniform distribution of length changes applied to frog muscle fibres. *J Physiol* 1979; 293: 379-392.
[10] Altringham, JD, and Bottinelli, R. The descending limb of the sarcomere length–force relation in single muscle fibres of the frog. *J Muscle Res Cell Motil* 1985; 6(5): 585-600.
[11] Granzier, HL, and Pollack, GH. The descending limb of the force-sarcomere length relation of the frog revisited. *J Physiol* 1990; 421: 595-615.
[12] Holzapfel, GA, and Ogden, RW. On the bending and stretching elasticity of biopolymer filaments. *J Elasticity* 2011; 104(1-2): 319–342.
[13] Winters, TM, Takahashi, M, Lieber, RL, and Ward, SR. Whole muscle length–tension relationships are accurately modeled as scaled sarcomeres in rabbit hindlimb muscles. *J Biomech* 2011; 44(1): 109-115.
[14] Hill, AV. The mechanics of active muscle. *Proc R Soc Lond B Biol Sci* 1953; 141(902): 104-117.
[15] Gordon, AM, Huxley, AF, and Julian, FJ. Tension development in highly stretched vertebrate muscle fibres. *J Physiol* 1966; 184(1): 143-169.
[16] Allinger, TL, Epstein, M, and Herzog, W. Stability of muscle fibers on the descending limb of the force–length relation. A theoretical consideration. *J Biomech* 1996; 29(5): 627-633.

[17] Zahalak, GI. Can muscle fibers be stable on the descending limbs of their sarcomere length-tension relations? *J Biomech* 1997; 30(11–12): 1179–1182.
[18] Horowits, R. The physiological role of titin in striated muscle. *Rev Physiol Biochem Pharmacol* 1999; 138: 57-96.
[19] Proske, U, and Morgan, DL. Muscle damage from eccentric exercise: mechanism, mechanical signs, adaptation and clinical applications. *J Physiol* 2001; 537(Pt 2): 333-345.
[20] Rice, JR (ed.). The localization of plastic deformation. In *14th International Congress on Theoretical and Applied Mechanics*. Delft: North Holland, 1976.
[21] Simha, N, and Truskinovsky, L. Phase diagram of zirconia in stress space. In: Batra, R (ed.), *Contemporary research in mechanics and mathematics of materials*. Barcelona: CIMNE, 1996; pp. 310-321.
[22] Telley, IA, Denoth, J, and Ranatunga, KW. Inter-sarcomere dynamics in muscle fibres. A neglected subject? *Adv Exp Med Biol* 2003; 538: 481-500; discussion
[23] Telley, IA, Stehle, R, Ranatunga, KW, Pfitzer, G, Stussi, E, and Denoth, J. Dynamic behaviour of half-sarcomeres during and after stretch in activated rabbit psoas myofibrils: sarcomere asymmetry but no 'sarcomere popping'. *J Physiol* 2006; 573(Pt 1): 173-185.
[24] Telley, IA, Denoth, J, Stussi, E, Pfitzer, G, and Stehle, R. Half-sarcomere dynamics in myofibrils during activation and relaxation studied by tracking fluorescent markers. *Biophys J* 2006; 90(2): 514-530.
[25] Stoecker, U, Telley, IA, Stussi, E, and Denoth, J. A multisegmental cross-bridge kinetics model of the myofibril. *J Theor Biol* 2009; 259(4): 714-726.
[26] Givli, S. Towards multi-scale modeling of muscle fibers with sarcomere non-uniformities. *J Theor Biol* 2010; 264(3): 882-892.
[27] Campbell, SG, Hatfield, PC, and Campbell, KS. A mathematical model of muscle containing heterogeneous half-sarcomeres exhibits residual force enhancement. *PLoS Comput Biol* 2011; 7(9): e1002156.
[28] Page, SG, and Huxley, HE. Filament lengths in striated muscle. *J Cell Biol* 1963; 19: 369-390.
[29] Iwazumi, T, and Pollack, GH. The effect of sarcomere non-uniformity on the sarcomere length-tension relationship of skinned fibers. *J Cell Physiol* 1981; 106(3): 321-337.
[30] Horowits, R, and Podolsky, RJ. The positional stability of thick filaments in activated skeletal muscle depends on sarcomere length: evidence for the role of titin filaments. *J Cell Biol* 1987; 105(5): 2217-2223.
[31] Morgan, DL, and Allen, DG. Early events in stretch-induced muscle damage. *J Appl Physiol (1985)* 1999; 87(6): 2007-2015.
[32] Brown, LM. An electron microscopists role in experiments on isolated muscle fibres. In: Simmons, RM (ed.), *Muscular Contraction*. Cambridge: Cambridge University Press, 1992; pp. 189-201.
[33] Morgan, DL. An explanation for residual increased tension in striated muscle after stretch during contraction. *Exp Physiol* 1994; 79(5): 831-838.
[34] Brown, LM, and Hill, L. Some observations on variations in filament overlap in tetanized muscle fibres and fibres stretched during a tetanus, detected in the electron microscope after rapid fixation. *J Muscle Res Cell Motil* 1991; 12(2): 171-182.
[35] Huxley, AF, and Peachey, LD. The maximum length for contraction in vertebrate straiated muscle. *J Physiol* 1961; 156: 150-165.
[36] Lieber, RL, and Baskin, RJ. Intersarcomere dynamics of single muscle fibers during fixed-end tetani. *J Gen Physiol* 1983; 82(3): 347-364.
[37] Morgan, DL, Whitehead, NP, Wise, AK, Gregory, JE, and Proske, U. Tension changes in the cat soleus muscle following slow stretch or shortening of the contracting muscle. *J Physiol* 2000; 522(Pt 3): 503-513.
[38] Abbott, BC, and Aubert, XM. The force exerted by active striated muscle during and after change of length. *J Physiol* 1952; 117(1): 77-86.
[39] Hill, L. A-band length, striation spacing and tension change on stretch of active muscle. *J Physiol* 1977; 266(3): 677-685.
[40] Edman, KA, Elzinga, G, and Noble, MI. Residual force enhancement after stretch of contracting frog single muscle fibers. *J Gen Physiol* 1982; 80(5): 769-784.
[41] Edman, KA, Caputo, C, and Lou, F. Depression of tetanic force induced by loaded shortening of frog muscle fibres. *J Physiol* 1993; 466: 535-552.
[42] Morgan, DL. New insights into the behavior of muscle during active lengthening. *Biophys J* 1990; 57(2): 209-221.
[43] Noble, MI. Enhancement of mechanical performance of striated muscle by stretch during contraction. *Exp Physiol* 1992; 77(4): 539-552.
[44] Edman, KA, and Tsuchiya, T. Strain of passive elements during force enhancement by stretch in frog muscle fibres. *J Physiol* 1996; 490(Pt 1): 191-205.
[45] Talbot, JA, and Morgan, DL. Quantitative analysis of sarcomere non-uniformities in active muscle following a stretch. *J Muscle Res Cell Motil* 1996; 17(2): 261-268.
[46] Wakeling, J, Herzog, W, and Syme, D (eds). Force enhancement and stability in skeletal muscle fibers. In: *XI Congress of the Canadian Society for Biomechanics*, Montreal, 2000.

[47] Epstein, M, and Herzog, W. Aspects of skeletal muscle modelling. *Philos Trans R Soc Lond B Biol Sci* 2003; 358(1437): 1445-1452.
[48] Edman, KA. Contractile performance of striated muscle. *Adv Exp Med Biol* 2010; 682: 7-40.
[49] Rassier, DE, and Pavlov, I. Contractile characteristics of sarcomeres arranged in series or mechanically isolated from myofibrils. *Adv Exp Med Biol* 2010; 682: 123-140.
[50] Edman, KA. Residual force enhancement after stretch in striated muscle. A consequence of increased myofilament overlap? *J Physiol* 2012; 590(Pt 6): 1339-1345.
[51] Ford, LE, Huxley, AF, and Simmons, RM. Tension responses to sudden length change in stimulated frog muscle fibres near slack length. *J Physiol* 1977; 269(2): 441–515.
[52] Ford, LE, Huxley, AF, and Simmons, RM. The relation between stiffness and filament overlap in stimulated frog muscle fibres. *J Physiol* 1981; 311: 219–249.
[53] Linari, M, Lucii L, Reconditi, M, Casoni, ME, Amenitsch, H, Bernstorff, S, et al. A combined mechanical and X-ray diffraction study of stretch potentiation in single frog muscle fibres. *J Physiol* 2000; 526(Pt3): 589–596.
[54] Pinniger, GJ, Ranatunga, KW, and Offer, GW. Crossbridge and non-crossbridge contributions to tension in lengthening rat muscle: force-induced reversal of the power stroke. *J Physiol* 2006; 573(Pt 3): 627–643.
[55] Minozzo, FC, and Rassier, DE. Effects of blebbistatin and Ca2+ concentration on force produced during stretch of skeletal muscle fibers. *Am J Physiol Cell Physiol* 2010; 299(5): C1127–C1135.
[56] Labeit, D, Watanabe, K, Witt, C, Fujita, H, Wu, Y, Lahmers S, et al. Calcium-dependent molecular spring elements in the giant protein titin. *Proc Natl Acad Sci USA* 2003; 100(23): 13716–13721.
[57] Joumaa, V, Rassier, DE, Leonard, TR, and Herzog, W. The origin of passive force enhancement in skeletal muscle. *Am J Physiol Cell Physiol* 2008; 294(1): C74–C78.
[58] Duvall, MM, Gifford, JL, Amrein, M, and Herzog, W. Altered mechanical properties of titin immunoglobulin domain 27 in the presence of calcium. *Eur Biophys J* 2012; 42(4): 301–307.
[59] Herzog, W, Duvall, M, and Leonard, TR. Molecular mechanisms of muscle force regulation: a role for titin? *Exerc Sport Sci Rev* 2012; 40(1): 50–57
[60] Herzog, W, Leonard, T, Joumaa, V, DuVall, M, and Panchangam A. The three filament model of skeletal muscle stability and force production. *Mol Cell Biomech* 2012; 9(3): 175-191.
[61] Rassier, DE. The mechanisms of the residual force enhancement after stretch of skeletal muscle: non-uniformity in half-sarcomeres and stiffness of titin. *Proc Biol Sci* 2012; 279(1739): 2705–2713.
[62] Minozzo, FC, and Lira, CA. Muscle residual force enhancement: a brief review. *Clinics (Sao Paulo)* 2013; 68(2): 269–274.
[63] Morgan, DL, Mochon, S, and Julian, FJ. A quantitative model of intersarcomere dynamics during fixed-end contractions of single frog muscle fibers. *Biophys J* 1982; 39(2): 189–196.
[64] Saldana, RP, and Smith, DA. Four aspects of creep phenomena in striated muscle. *J Muscle Res Cell Motil* 1991; 12(6): 517–531.
[65] Denoth, J, Stüssi, E, Csucs, G, and Danuser, G. Single muscle fiber contraction is dictated by inter-sarcomere dynamics. *J Theor Biol* 2002; 216(1): 101-22.
[66] Puglisi, G, and Truskinovsky, L. Mechanics of a discrete chain with bi-stable elements. *J Mech Phys Solids* 2000; 48(1): 1-27.
[67] Aubry, S, and LeDaeron, P. The discrete Frenkel–Kontorova model and its extensions: I. Exact results for the ground-states. *Physica D* 1983; 8(3): 381-422.
[68] Marcucci, L, and Truskinovsky, L. Muscle contraction: A mechanical perspective. *Eur Phys J E Soft Matter* 2010; 32(4): 411–418.
[69] Sheshka, R, and Truskinovsky, L. Power-stroke-driven actomyosin contractility. *Phys Rev E Stat Nonlin Soft Matter Phys* 2014; 89(1): 012708.
[70] Katz, B. The relation between force and speed in muscular contraction. *J Physiol* 1939; 96(1): 45-64.
[71] Hill, AV. The heat of shortening and the dynamic constants of muscle. *Proc Roy Soc Lond* 1938; 126: 136-195.
[72] Bischofs, LB, and Schwarz, US. Force-dependent kinetics of focal adhesions determines cell organization in soft media. *Biophys J* 2004; 86(1): 58a-59a.
[73] Schwarz, US, and Safran, SA. Physics of adherent cells. *Rev Mod Phys* 2013; 85(3): 1327–1381.
[74] Rogers, RC, and Truskinovsky, L. Discretization and hysteresis. *Physica B* 1997; 233(4): 370–375.
[75] Truskinovsky, L, and Vainchtein, A. The origin of nucleation peak in transformational plasticity. *J Mech Phys Solids* 2004; 52(6): 1421-1446.
[76] Rassier, DE, and Herzog, W. Effects of shortening on stretch-induced force enhancement in single skeletal muscle fibers. *J Biomech* 2004; 37(9): 1305–1312.
[77] Peterson, DR, Rassier, DE, and Herzog, W. Force enhancement in single skeletal muscle fibres on the ascending limb of the force-length relationship. *J Exp Biol* 2004; 207(Pt 16): 2787–2791.

[78] Sugi, H, and Tsuchiya, T. Stiffness changes during enhancement and deficit of isometric force by slow length changes in frog skeletal muscle fibres. *J Physiol* 1988; 407: 215–229.
[79] Aubry, S. Exact models with a complete Devil's staircase. *J Phys C Solid State Phys* 1983; 16(13): 2497–2508.
[80] Edman, KA, Elzinga, G, and Noble, MI. Enhancement of mechanical performance by stretch during tetanic contractions of vertebrate skeletal muscle fibres. *J Physiol* 1978; 281: 139-155.
[81] Rief, M, Gautel, M, Oesterhelt, F, Fernandez, JM, and Gaub, HE. Reversible unfolding of individual titin immunoglobulin domains by AFM. *Science* 1997; 276(5315): 1109–1112.
[82] Herzog, W, and Leonard, TR. Force enhancement following stretching of skeletal muscle: a new mechanism. *J Exp Biol* 2002; 205(Pt 9): 1275-1283.